Measurements and Models for 38-GHz Point-to-Multipoint Radiowave Propagation

Hao Xu, *Student Member, IEEE*, Theodore S. Rappaport, *Fellow, IEEE*, Robert J. Boyle, and James H. Schaffner, *Senior Member, IEEE*

***Abstract*—This article presents results of a wide-band measurement campaign conducted at 38 GHz. The objective of the research was to determine multipath and time varying channel behavior of short-hop millimeter-wave point-to-multipoint radio links during various weather events. 73 963 power delay profiles (PDP's) were captured on three links, each comparable to proposed local multipoint distribution systems (LMDS) in a campus environment. Multipath was observed in unobstructed LOS links during rain but not during clear weather. Short-term variation of the received signal over 1–2 min observation periods is described by a Rician distribution with a K factor which varies as a function of rain rate. Measured rain attenuation exceeds Crane Model predictions by several decibels.**

A novel prediction technique is presented that applies canonical antenna patterns and site specific information to estimate worst case multipath channel characteristics including relative power, time of arrival (TOA), and angle of arrival (AOA) of each multipath component. New metrics, the *excess delay zone* and *relative power zone*, are defined and contour plots are developed to determine potential reflectors from an area site map. These results and models provide useful guidelines for the design of millimeter-wave wireless communication systems.

***Index Terms*—38 GHz, LMDS, MBS, millimeter-wave propagation, rain attenuation.**

I. Introduction

THE INCREASING demand for broadband multimedia communications coupled with new millimeter-wave spectrum issued by governments throughout the world has motivated extensive research in new wireless services such as local multipoint distribution systems (LMDS), mobile broadband systems (MBS), and next generation internet (NGI). Applications include video distribution, teleconferencing, last mile internet access, and wireless local loop telephony (WLL) [1], [2].

The millimeter-wave band is uniquely suited for these services because of the large available bandwidth, high-frequency reuse, and the reduced size of radiating and receiving antennas and electronic components. The design of a high-performance broadband millimeter-wave communication system requires detailed knowledge of radio wave propagation channel. At frequencies above 10 GHz, one must not only consider classical propagation phenomena such as reflection, diffraction, and scattering, but also the interaction of electromagnetic waves with the atmosphere, and particles such as rain, snow, and hail [3], [4].

Research for broadband terrestrial propagation channel at microwave- and millimeter-wave frequencies has been reported for the past several decades. W. D. Rummler developed microwave line-of-sight (LOS) propagation model from extensive power measurements on a 42.5 km hop at 6 GHz [5]. An initial study for LMDS systems has been reported in [6], where multipath, signal attenuation, depolarization, and cell-to-cell coverage issues were studied. Path loss and the presence of specular reflections as a function of antenna height were studied for LMDS environments in [7]. In [8], narrowband and wide-band measurements were performed on point-to-point transmission at street level at upper microwave- and lower millimeter-wave bands of 9.6, 28.8, and 57.6 GHz for narrowband measurements, and 30.3 GHz for wide-band measurements. Research on propagation through vegetation has been reported in [9] for 9.6, 28.8, and 57.6 GHz, and in [10] for 9.6, 28.8, 57.6, and 96.1 GHz. However, none of these works studied the effects of weather on the channel. Rain attenuation has been studied by Crane [4] and others [11]–[14]. Although the rain attenuation and depolarization effects were studied in detail, no research has addressed the effects of rain on the wide-band multipath behavior of the channel.

This paper presents one of the first studies of wide-band (200-MHz RF bandwidth) propagation under different weather conditions at millimeter-wave frequencies over short links. The measurement campaign was conducted from April to June 1998, via three cross-campus links at Virginia Tech [15]. These links represent typical LMDS links with various levels of obstructions due to vegetation. Specifically, these links provided an unobstructed path, a partially obstructed path, and a completely obstructed path by vegetation.

The measurement campaign produced a variety of results including average rain attenuation, short-term signal variation during rain, attenuation through glass and vegetation, and wide-band power delay profiles (PDP's). Received signal during rain is described by the average power and Rician probability density function (pdf). The relationship between Rician K factor and rain rate shows the increase of the incoherent power and the decrease of the coherent power during heavy rain. The observed multipath propagation via an unobstructed LOS link during rain may be the result of two physical

Manuscript received February 16, 1999; revised September 30, 1999. This work was supported by Hughes Network Systems, HRL, and the Mobile and Portable Radio Research Group (MPRG) of Virginia Tech.

H. Xu, T. S. Rappaport, and R. J. Boyle are with the Mobile and Portable Radio Research Group, Bradley Department of Electrical and Computer Engineering, Virginia Tech, Blacksburg, VA 24061, USA (e-mail: haoxu@vt.edu).

J. H. Schaffner is with HRL Laboratories, Malibu, CA 90265 USA (e-mail: jhschaffner@HRL.com).

Publisher Item Identifier S 0733-8716(00)01297-X.

mechanisms: atmospheric inhomogeneities or changes in the electromagnetic properties (i.e., reflectivity) of the surrounding scatterers, such as building surfaces.

Based on the measurement results, a novel technique has been developed to estimate the worst case power, excess delay, and angle of arrival of a multipath component for any given antenna beam patterns. These multipath parameters are estimated using *excess delay contour plot* and the *relative power contour plot*, which are developed using antenna patterns and the geometry associated with the link. These contour plots allow wireless engineers to quickly determine the worst case multipath channel response based on site-specific information.

Section II describes the hardware of the measurement system used to conduct the wide-band path loss and PDP measurements. Section III discusses the experimental setup and measurement site information. Section IV presents the results of the measurement campaign and the empirical models derived from the measurements. Section V describes a novel prediction technique for multipath characteristics of a millimeter-wave communications link. Section VI presents conclusions from this work.

II. Measurement System Hardware

Typical LMDS systems consist of a transmitting station (a hub) with a sectorized or wide beam antenna and a receiver (a subscriber) with a highly directional antenna. To recreate such a link, a sector horn transmitting antenna and a parabolic reflector receiving antenna were used in the measurement campaign. These antennas have been proposed for commercial 38 GHz LMDS. Table I summarizes the antenna information, where d_F is the far-field *Fraunhofer distance.* Care was taken to ensure that the transmitter and receiver antennas remained in their respective far fields throughout the measurement campaign.

A *spread spectrum sliding correlator channel sounder* was used to measure the channel PDP's [16]. The channel sounder, which was originally designed for frequencies up to 5.85 GHz [17], was upgraded by the authors to operate at 38 GHz [18]. The block-diagram of the system is shown in Fig. 1, where an intermediate frequency (IF) of 5.4 GHz was used as part of an upconverter system with an RF output of 37.8 GHz. Note that 10-MHz Rubidium oscillators were used to drive both the pseudonoise (PN) sequence generators and the IF clocks.

Parameters for the sliding correlator system were carefully selected to optimize measurement performance. The effective isotropically radiated power (EIRP) was 40 dBm. The PN sequence clock rate was set to a value of 100 MHz, which provided a 10 ns time resolution, and a 200-MHz null-to-null RF bandwidth. The frequency offset between the transmitter and receiver PN clock was set to 100 KHz (i.e., a sliding factor of 1000) in order to provide a good compromise between measurement system speed and multipath dynamic range. In this configuration, the measurement system provided 50 PDP's per second and a multipath dynamic range of 25 dB. Switches were built into the measurement apparatus to change from wide-band measurement mode into continuous-wave (CW) measurement mode for antenna alignments and calibration.

TABLE I
ANTENNA INFORMATION SUMMARY

	Type	3 dB beamwidth		d_F	Gain	Polarization
		Azimuth	Elevation	(m)	(dB)	
Transmitter	Horn	45^0	6.5^0	1.02	19	Vertical
Receiver	Parabolic	1.5^0	1.5^0	23.6	39	Vertical

At each measurement site, received CW power levels were recorded every hour to verify the system stability. Also, *free space calibration* via an 30.5 m (100 ft) LOS link during clear weather conditions was performed to verify the performance of the hardware system. The difference between the theoretical path loss and measured path loss was less than 1 dB.

Careful records of rain ware taken every minute using a tipping bucket rain gauge with a resolution of 15.24 mm/h. The rain gauge was located on the rooftop at the transmitter or receiver site. It was assumed that the rain rate was relatively constant along the short links of less than 1 km. Results from [4] show that small rain cell sizes are on the order of 5 km^2. Weather data files and measured channel responses were time stamped in order to establish a one-to-one correspondence between the channel PDP measurements and the recorded weather conditions.

III. Measurement Setup

A. Point-to-Point Link Description

The summary of three cross-campus point-to-point links is listed in Table II. Their geometry is shown in Figs. 2 and 3. The first link, L1, provided a 605 m unobstructed LOS path. The second link, L2, provided a 262 m obstructed path, where the LOS path was obstructed by the dense canopy of a big oak tree. The third link, L3, provided a 262 m partially obstructed path, where the leaves of an oak tree were sufficiently close to the LOS path, that they could partially obstruct the LOS path during windy weather conditions.

For measurements via these links, the transmitter and receiver were both located indoors and were left to run continuously. This is essential to maintain antenna alignment, constant gain, and to capture sudden weather changes. Care was taken to measure the attenuation through the window glass (Section IV-E).

For each link, the equipment was turned on for at least 30 min before any measurements to reduce thermal drift. Then CW power measurements were performed for system calibration and antenna alignment between transmitter and receiver. The measurement system was then switched to *sliding correlator measurement mode* and PDP's were recorded at the receiver through each day during various weather conditions.

B. Attenuation Measurements

Excess attenuation due to tree, glass and weather events were measured with respect to free space path loss. In free space, the received signal power, P_r, via an unobstructed LOS path with no multipath is given by

$$P_r(\text{dBm}) = P_t(\text{dBm}) + G_t(\text{dB}) + G_r(\text{dB}) - 20\log\frac{4\pi d}{\lambda}(\text{dB}) \quad (1)$$

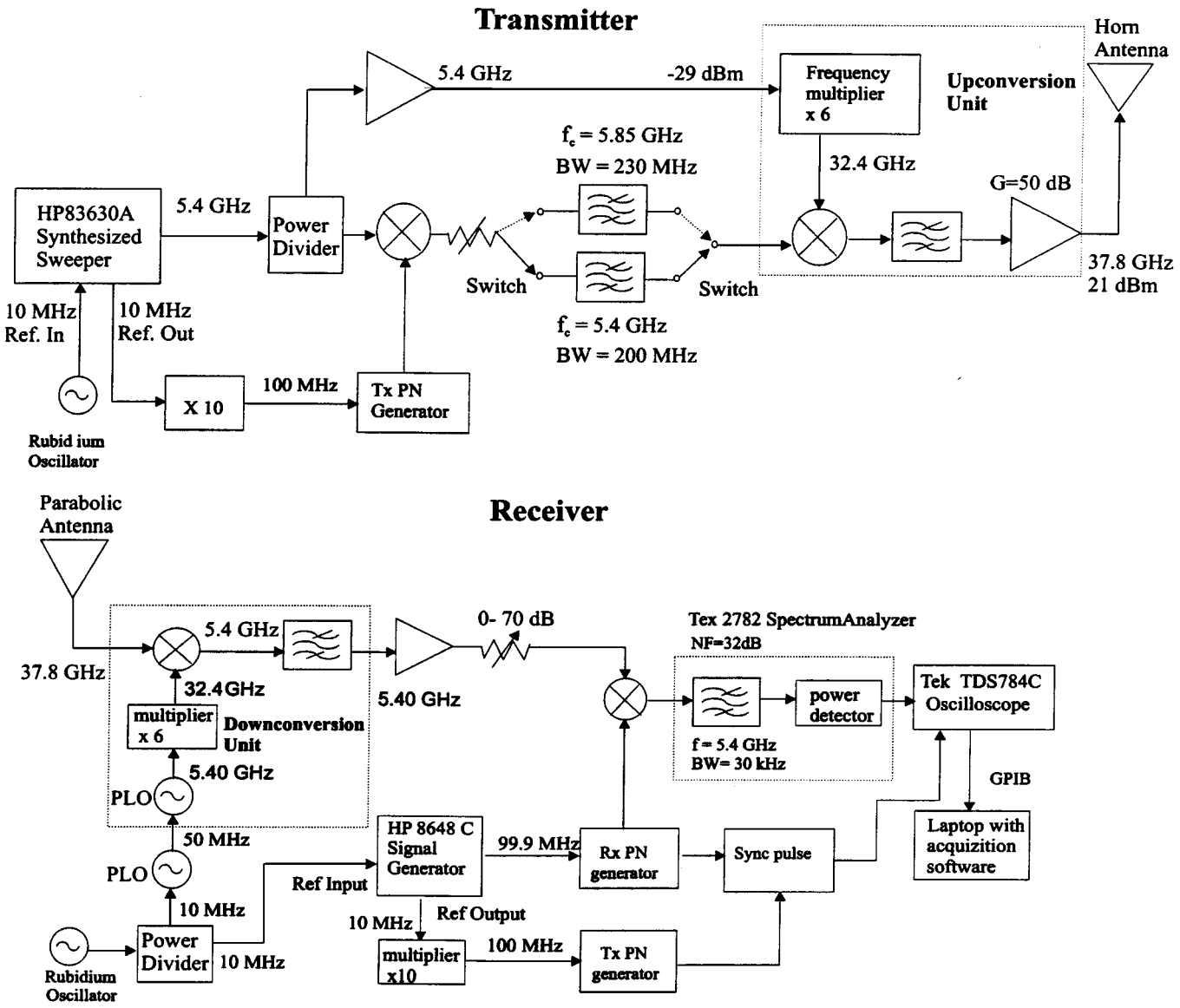

Fig. 1. Block-diagram of 38 GHz sliding correlator channel sounder.

where

P_t transmitted power;

G_t transmitter gains;

G_r receiver gains;

λ wavelength;

d path length.

If an obstruction is present, then the received signal will suffer additional attenuation. Equation (2) accounts for additional attenuation mechanisms caused by the channel, where PL_x denotes the path loss induced by obstruction "x"

$$P_r(\text{dBm}) = P_t(\text{dBm}) + G_t(\text{dB}) + G_r(\text{dB}) - 20\log\frac{4\pi d}{\lambda} - PL_{\text{tree}} - PL_{\text{rain}} - PL_{\text{glass}}. \quad (2)$$

Equations (1) and (2) were used to measure attenuation due to rain, hail, tree leaves, and window glass.

C. Time Dispersion and Short Term Variation Measurements

Time dispersion of the channel is caused by multipath components arriving at the receiver with different excess delays and plays a major role in the design of equalizer for high-speed wireless modems. To measure channel time dispersion, the bandwidth of the channel sounder must exceed the channel coherence bandwidth. This ensures that all significant multipath components can be resolved and recorded in a PDP.

Short term variation of the received signal is caused by the dynamic nature of the channel. Temporal variations in the channel result from various factors including randomly moving objects (such as tree leaves), changes in surface roughness of scatterers, and meteorological particles (such as falling raindrops). These channel dynamics drive many wireless modem specifications. For example, the update rate of an adaptive equalizer must exceed the Doppler spread of the channel so that its tap weights track the channel variations.

To measure channel dynamics, the sampling rate of channel measurement system must exceed twice the Doppler spread of

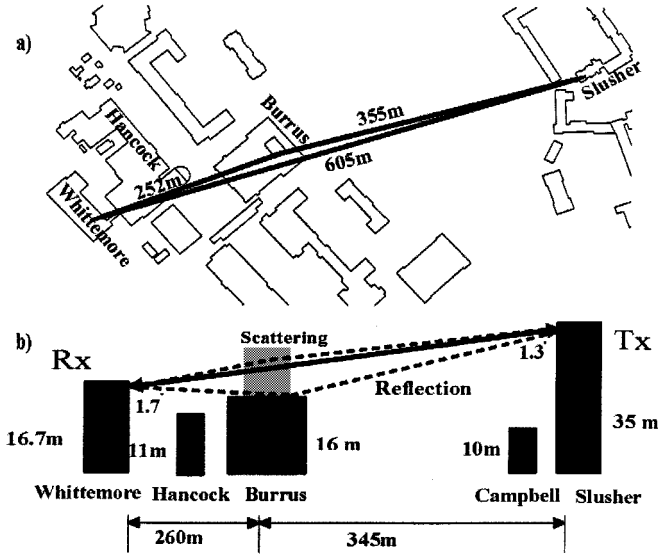

Fig. 2. Geometry of the Slusher–Whittemore link—605 m unobstructed LOS Link (L1). (a) Top view. (b) Side view.

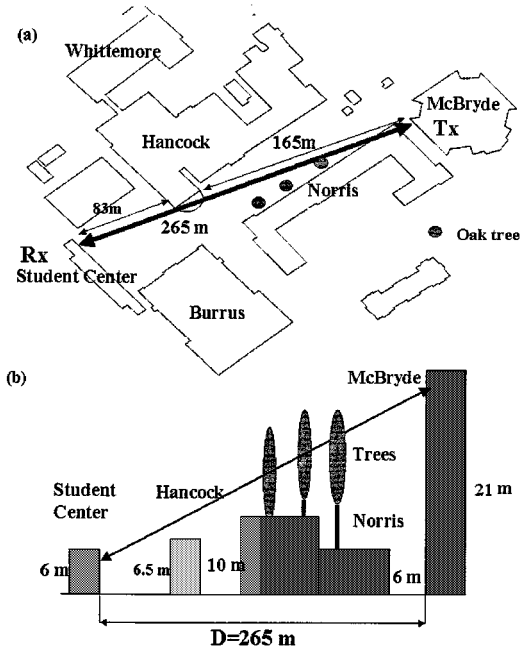

Fig. 3. Geometry of the McBryde-Student Center links—265 m obstructed LOS link (L2) and partially obstructed LOS link (L3). (a) Top view. (b) Side view.

the channel. In this campaign, the system speed is 50 PDP's per second, and has the capability of tracking short term variations for very low Doppler spread. For rapidly time-varying situations, higher channel sampling rates are required. On the other hand, rapidly sampled CW measurements can capture the high-speed channel dynamics.

D. Controlled Reflection Measurements

wide-band measurements via the unobstructed LOS link show multipath during rain. This multipath may be caused by the change in the electromagnetic properties of nearby building surfaces as they become wet. To investigate this phenomenon,

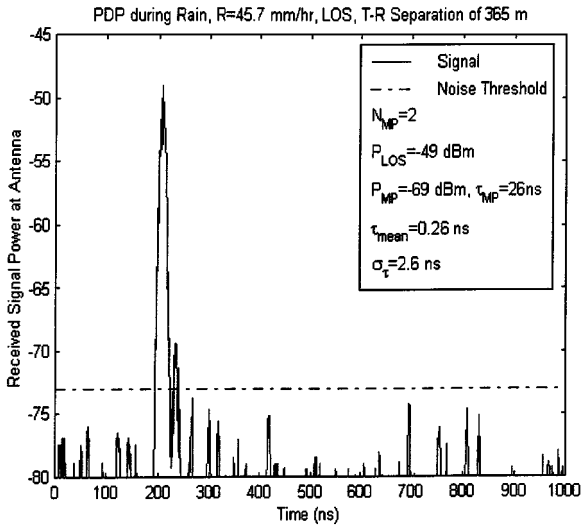

Fig. 4. Typical PDP under rainy conditions: May 3, 265 m unobstructed LOS link, rain rate of 45.72 mm/h.

controlled reflection measurements were conducted for glass and brick surfaces.

For each surface, specular reflected waves were measured for five incident angles of 15, 30, 45, 60, and 80°. Before the measurement, a free space calibration was carried out. Then, the transmitter and receiver antennas were aimed at the surface under study, and the measured received power was compared to the calibrated free space power. For each angle, the received power was first recorded for the dry wall. The wall was then soaked with water for three minutes, and the received power was again recorded. Due to the inherent limitation of our vertically polarized antennas, only reflection coefficients for the perpendicular polarization (the electric field is perpendicular to plane of incidence) were measured.

The front entrance of the new engineering building was chosen for the glass reflection measurements. The transmitter was located 6.1 m from the glass, and receiver was 24.4 m from the glass. A side wall of Shultz Hall was chosen for the brick reflection coefficient measurements. The transmitter and the receiver were located 15.2 and 30.5 m from the brick wall, respectively.

IV. Measurement Results and Statistical Channel Models

A total of 73 963 PDP's were recorded for the three cross-campus links. An example of a PDP is presented in Fig. 4. Each PDP was processed to determine the number of multipath components above the noise threshold, N_{MP}; the power of the LOS component, P_{LOS}; the power and excess delay time of each multipath component, P_{MP}, and τ_{MP}; the mean excess delay, τ_{mean}; and RMS delay spread, σ_τ. Statistical results are summarized in the following sections.

A. Channel Multipath Characteristics

1) Multipath Channel Measurement Result Summary: For all of the seven rainy days, statistics of multipath occurrence is

TABLE II
WIDEBAND POINT-TO-POINT LINKS SUMMARY

Locations	T-R (m)	h(Tx) (m)	h(Rx)(m)	Clearance	Dates
L1: Slusher-Whittemore	605	663	645	LOS	4/22-5/3
L2: McBride-GBJ *	265	652	637	Obstructed Path	5/13-5/27
L3: McBride-GBJ *	265	652	637	Partially Obstructed Path	5/27-6/9

*:two transmitter locations for McBride-GBJ path

h(Tx) and h(Rx) are transmitter and receiver heights above sea level

summarized in Table III, and statistics of multipath parameters is summarized in Table IV.

In Table III, recorded PDP's are grouped by links, measurement date, and weather condition. For each group, multipath statistics are analyzed for different threshold levels, defined as the multipath component power with respect to the LOS component, P_{MP}–P_{LOS}. For each threshold, the percentage of the PDP's that contains at least one multipath component that exceeds this threshold is calculated.

For path L1, results show no multipath under clear conditions. This is expected, since the specular reflected wave is reduced due to the rough surface scattering, and the reflected waves with large AOA are rejected by the directional antennas. However, multipath was observed during rain. On May 3, during moderate rain, a few multipath components were detected at least 14 dB below LOS. On May 1, strong multipath components were detected during heavy rain right before and after a strong hailstorm passed through the link. In 53% of the PDP's taken right before and after the hailstorm, a multipath component was detected 12 dB below the LOS component. During the hailstorm, the power of LOS component was reduced by 25 dB, and multipath was observed in only one PDP out of 58 measured PDP's.

For path L2 and L3, few multipath components were detected under clear conditions. This was due to the scattering leaves between the LOS link. Like in the unobstructed LOS link, more multipath components were detected during rain events. Results from these three links indicate that severe weather conditions and vegetation near LOS path may cause multipath. Further discussions of relationship between weather and multipath is presented in Section IV-A2.

In Table IV, statistics on mean excess delay and RMS delay spread are presented both in average and maximum for all the PDP's that contain multipath components. Also, maximum multipath level is calculated with respect to the LOS component. Results show that, during rain, the RMS delay spread can be as high as 9.7 ns on an unobstructed LOS path, and 15.9 ns on an obstructed path.

2) Weather Effects on Multipath Characteristics: Wide-band measurements showed significant changes in multipath characteristics during certain weather events. A comparison of the PDP's under different weather conditions is presented in Fig. 5. All three PDP's were collected from L1. Although no multipath component was detected under clear conditions, multipath component was detected about 16 dB below LOS during the light rain on May 3, and 12 dB below LOS during the moderate rain before the hailstorm on May 1. On May 3, the small multipath components remained after the rain until the building surfaces dried up.

Two hypotheses may explain the presence of these multipath components. The first one is based on inhomogeneities in the

TABLE III
SUMMARY OF MULTIPATH OCCURRENCE VIA THREE LINKS: L1–LOS, 605 m; L2–partially obstructed path, 265 m; L3–obstructed path, 265 m

Link	Date	R(mm/h)	# PDPs	minutes	% of PDPs with multipath > ΔP				
Threshold:$\Delta P = P_{MP} - P_{LOS}$(dB)					-10	-12	-14	-16	-18
L1	4/23	clear	190	2	0	0	0	0	0
		0–15.2	100	1	0	0	0	0	0
	5/1	0–39.6	60	3	1.7	53	67	67	67
		hail	58	1	1.7	1.7	1.7	1.7	6.9
	5/3	clear	10	4	0	0	0	0	0
		0–45.7	620	15	0	0	0	3.7	27
L2	5/27	clear	4400	8	0.068	0.14	0.20	1	27
		0–15.2	3000	3	0.83	2.4	8.6	21	28
L3	5/30	clear	800	2	0.25	0.25	0.25	0.25	21.8
		0–15.2	8350	12	0.08	0.12	0.74	7.7	21
	6/2	clear	7550	4	0.066	0.066	0.066	0.12	0.49
		0–213.4	16850	24	0.17	0.22	0.81	4.7	17.6
	6/3	clear	2000	4	0.05	0.05	0.55	11	52
		0–45.72	4300	6	0.047	0.047	0.12	1.8	11

TABLE IV
MEAN EXCESS DELAY, RMS DELAY SPREAD AND MAXIMUM MULTIPATH (MP) LEVEL (W.R.T. LOS) FROM PDP'S CONTAINING MULTIPATH COMPONENTS

Link	Date	R(mm/hr)	$\overline{\tau}$ (ns)	τ_{max} (ns)	$\overline{\sigma}$ (ns)	σ_{max} (ns)	Max MP(dB)
L1	5/1	40	1.7	3.1	6.4	9.7	-9.1
		Hail	0.64	2.31	3.4	6.61	-5.2
	5/3	0–45.7	0.5	3.5	3.5	6.1	-14.2
L2	5/27	clear	0.7	5	3.9	8.1	-9.0
		< 15.2	1.43	9.9	7.5	15.4	-9.3
L3	5/30	clear	0.4	2.8	4.2	5.9	-4.5
		< 15.2	0.7	9.1	5.3	15.9	-4.75
	6/2	clear	0.4	3.4	4.1	7.8	-3.1
		0–213	0.7	5.3	5.3	10	-2.6
	6/3	clear	0.8	2.5	5.9	9.9	-6.9
		0–213	0.36	4.2	3.2	9.7	-1.4

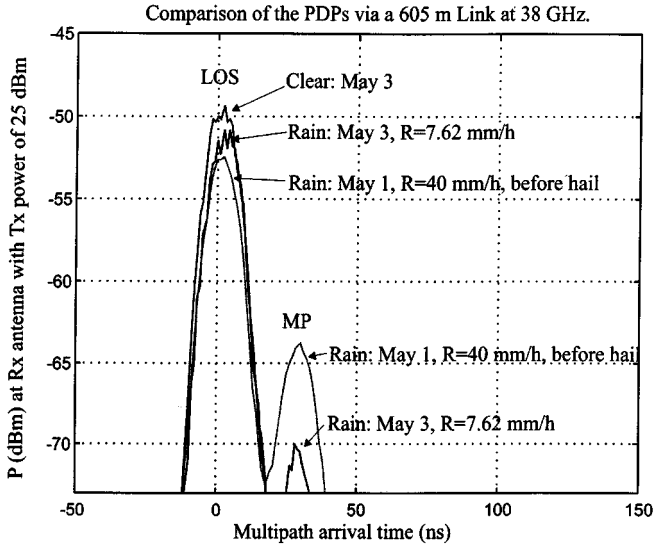

Fig. 5. Comparison of PDP's under different weather conditions: 605 m unobstructed LOS link.

atmosphere. Multipath components that occurred right before and after the hailstorm may be caused by the sharp edge of the hailstorm cell, which was illuminated by the antenna main lobe or first side lobe. In [19], de Wolf and Ligthart showed that multipath could occur at the edges of very intense and compact rain cells. Pressure, temperature, and rain could alter the refractivity of the atmosphere, thus creating varying propagation paths and propagation delays.

The second hypothesis is based on the change of the electromagnetic properties of the surface or the formation of standing water surfaces during rain. The rough surface on the rooftop of Burruss Hall would diffusively scatter the incoming wave during dry conditions. However, if the surface becomes wet or standing water surface forms during a rain event, the reflected power in the specular direction would increase. Multipath components remained after rain, which seems to support this hypothesis.

Controlled reflection measurements were conducted to investigate the change of the specular reflected power from brick and glass surfaces under wet and dry conditions. Brick wall measurements showed that the reflected power of wet walls was 0.02 to 3.5 dB higher than the reflected power of dry walls. Similar results were found for glass walls, where the difference was as high as 6.8 dB.

B. Short-Term Variation

The measurement speed of 50 PDP's per second enables the measurement system to take a huge amount of data during a short period of time and track the channel dynamics. Results from Fig. 6 show a wide variation of the received signal power at constant rain rates. This section analyzes the signal variation at constant rain rates.

During rain, the received signal can be modeled as the sum of a constant (coherent) component, and randomly scattered (incoherent) components resulting from rain or other scatterers. Therefore, the resulting received signal is expected to follow a Rician distribution.

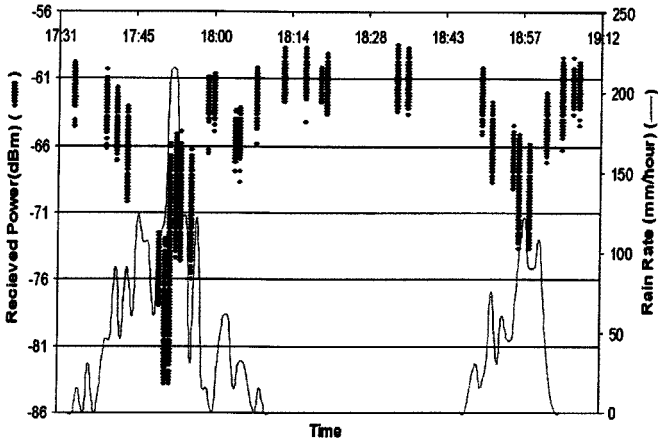

Fig. 6. Rain attenuation measurements: June 2, 265 m partially obstructed LOS link.

Rician pdf for the received signal envelop, $f_V(v)$, is [20]

$$f_V(v) = \frac{v}{\sigma^2} \exp\left\{-\frac{v^2 + A^2}{2\sigma^2}\right\} I_0\left(\frac{Av}{\sigma^2}\right) \tag{3}$$

where

v	signal envelop
$A^2/2$	coherent power;
σ^2	incoherent power;
$I_0(\cdot)$	modified Bessel function of the first kind and zero-order.

The Rician pdf is typically used to model the received envelop in a wireless channel that has LOS. The pdf for the received power, $P = V^2/2$, is then given by

$$f_P(p) = \frac{1}{\sigma^2} \exp\left\{-\frac{2p + A^2}{2\sigma^2}\right\} I_0\left(\frac{A\sqrt{2p}}{\sigma^2}\right). \tag{4}$$

Histograms of the received power at constant rain rate over short periods of 1–2 min are well described by (4). An example of measured and theoretical pdf from (4) is shown in Fig. 8(a).

Further, the mean and standard deviation of the received power from the measured data can be used to estimate Rician parameters A and σ, and coherent and incoherent powers. By definition, the mean received power, μ_p, and standard deviation, σ_p^2, are given by

$$\mu_p = E\{p\} = \int_0^\infty p f_P(p)\, dp = \sigma^2 + A^2/2 \tag{5}$$

$$E\{p^2\} = \int_0^\infty p^2 f_P(p)\, dp = 2\sigma^4 + 2A^2\sigma^2 + A^4/4 \tag{6}$$

$$\sigma_p = E\{p^2\} - E^2\{p\} = \sigma^4 + A^2\sigma^2 \tag{7}$$

where $E\{\bullet\}$ denotes ensemble average. From (5) and (7), σ and A can be solved from measured μ_p and σ_p.

Rician distribution can also be parameterized by total power and K factor, defined as the ratio of coherent to incoherent powers in dB. Using μ_p and σ_p from (5) and (7), K is computed as follows:

$$K = 10\log_{10}\frac{A^2/2}{\sigma^2} = 10\log_{10}\frac{\sqrt{\mu_p^2 - \sigma_p^2}}{\mu_p - \sqrt{\mu_p^2 - \sigma_p^2}}\ \text{dB}. \tag{8}$$

Equation (8) shows that the K factor is independent from the total received power. Therefore, the received power is normalized before calculating K. The resulting K factors for different rain rates are presented in Fig. 8(b). A minimum means square error (MMSE) fit is applied to the data, which leads to the following relationship between the Rician K factor (dB) and rain rate R (mm/h) as

$$K = 16.88 - 0.04R \text{ dB}. \tag{9}$$

Equation (9) shows that the K factor is proportional (with a negative sign) to rain rate. This is expected because as the rain rate increases, the coherent power decreases and the incoherent scattered power increases. The PDP's (Fig. 5) indeed show a decrease of the LOS power as the multipath power increases during rain.

Equation (9), combined with the received total power estimate, provides a powerful tool to model received signal variation and the resultant outage probability for LMDS systems. For a given rain rate and path length, the total received power can be estimated from (14) or (15) [Section IV-C, and K factor can be determined by (9)]. Coherent power, incoherent power, and the pdf of received power can be modeled accurately using the models described in this section.

C. Average Rain Attenuation

Fig. 6 shows an example of measured rain attenuation versus rain rate. Measurements were taken on June 2 from 17:30 to 19:30 during a heavy rain storm in Blacksburg, VA. The rain attenuation was as high as 26 dB at the rain rate of 213 mm/h. The received signal power displays a strong correlation with rain rate. A summary of average rain attenuation versus rain rate is provided in Fig. 7. Further, the measured rain attenuation is compared with the Crane prediction model.

The Crane model estimates the median rain attenuation based on rain rate, polarization and path length. It is a theoretical prediction model based on the geophysical observations of rain rate, rain structure, and the vertical variation of atmospheric temperature. The model is summarized in (10)–(13) [4]

$$A_R = aR^b \left[\frac{e^{ubd} - 1}{ub}\right] \quad (\text{for } 0 \le D \le d) \tag{10}$$

$$= aR^b \left[\frac{e^{ubd} - 1}{ub} - \frac{B^b e^{cbd}}{cb} + \frac{B^b e^{cbD}}{cb}\right] \quad (\text{for } d \le D \le 22.5 \text{ km}) \tag{11}$$

where

$$u = \ln[Be^{cd}]/d; \qquad B = 2.3R^{-0.17} \tag{12}$$

$$c = 0.026 - 0.03\ln(R); \qquad d = 3.8 - 0.6\ln(R) \text{ km} \tag{13}$$

and

A_R path attenuation due to rain in decibels;
R point rate in mm/h;
D path distance in kilometers.

For paths longer than 22.5 km, the attenuation A_R is calculated for a 22.5 km path, and the resulting rain outage time is multiplied by a factor of $(D/22.5)$. Multipliers a and b are rain attenuation coefficients, which are functions of frequency and polarization.

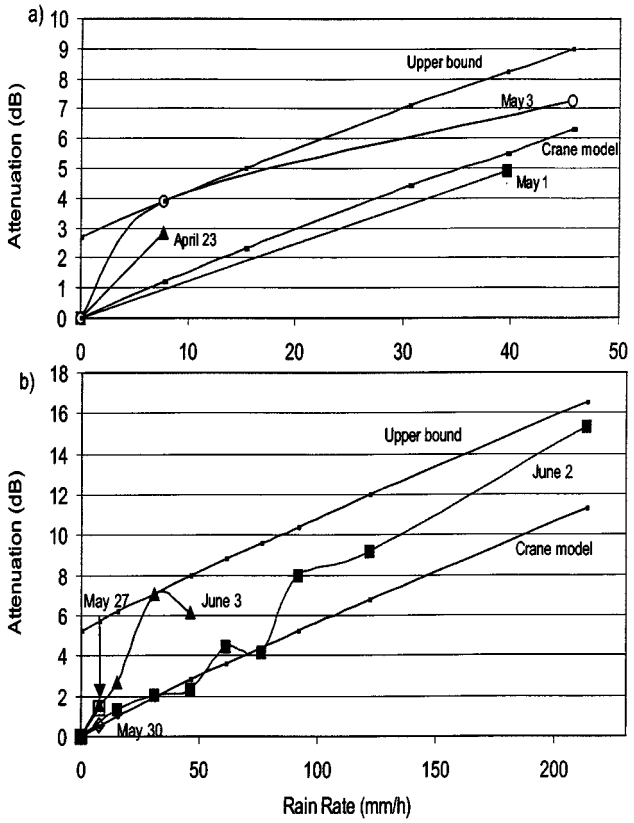

Fig. 7. Rain attenuation summary and upper bounds: (a) 605 m unobstructed LOS link and (b) 265 m partially obstructed and obstructed LOS links.

As shown in Fig. 7, our measurement results show slightly higher attenuation than the Crane model prediction. For link L1, where unobstructed LOS exists, the difference between the Crane model and our measurements is within 2.7 dB. For links L2 and L3, this difference increases to 5.2 dB.

The measurement results give rise to upper bounds for rain attenuation, (14) and (15), for an unobstructed LOS path and a partially obstructed LOS path, respectively

$$P^{\text{LOS}}_{\text{upperbound}}(R, D) = P_{\text{crane}}(R, D) + 2.7 \text{ (dB)} \tag{14}$$

$$P^{\text{partialLOS}}_{\text{upperbound}}(R, D) = P_{\text{crane}}(R, D) + 5.2 \text{ (dB)} \tag{15}$$

where

P_{crane} attenuation estimate based on the Crane model;
R (mm/h) rain rate;
D (m) path length.

These bounds provide a simple relationship between excess path attenuation, rain rate, and path length for short-haul links. The upper bound for partial obstructed LOS path provides an attenuation estimate that accounts for both rain and foliage.

D. Hail Attenuation

On May 1, a hailstorm passed through link L1. The hailstorm was preceded by light rain, then followed by heavy rain. The hailstorm lasted for two minutes and the hail size ranged from 0.5 to 1.5 cm in diameter. A total of 118 PDP's were measured before and during the hailstorm. The results of the rain and hail attenuation for May 1 are shown in Fig. 9. Comparison with the

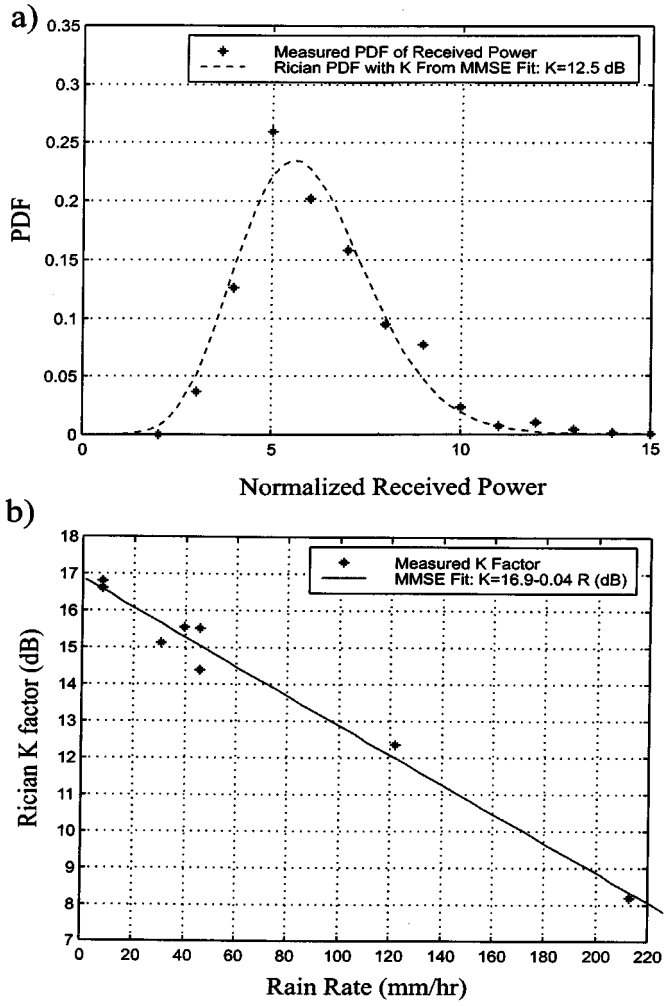

Fig. 8. Rain attenuation distribution: June 2, 265 m partially obstructed LOS link, rain rate of 122 mm/h.

reference power of –47 dBm under clear conditions shows that the hailstorm resulted in attenuation as high as 25.7 dB, and a signal variation of 7 dB over the 605 m path.

E. Glass and Tree Attenuation

To measure the attenuation of dry glass, the receiver was set up in the Johnson Student Center, and the transmitter was placed outside the building with only the window glass between them. Comparison of the received power through the glass with the received power in free space shows that the attenuation due to the glass is 25.5 dB. The glass measured is a double-pane, tempered and tinted window glass. Furthermore, comparison of the received signal power before rain (with dry glass) and immediately after rain (with rain drops still on the glass) showed less than 1 dB path loss difference, which indicates negligible attenuation due to rain drops on the glass.

As shown in Fig. 3, there is a row of oak trees in front of the Norris hall. Tree attenuation was estimated from measurements via two point-to-point links between McBryde Hall and Johnson Student Center. The path lengths for these two links were the same, with the only difference being whether or not the tree leaves blocked the LOS path. Measurements were taken during

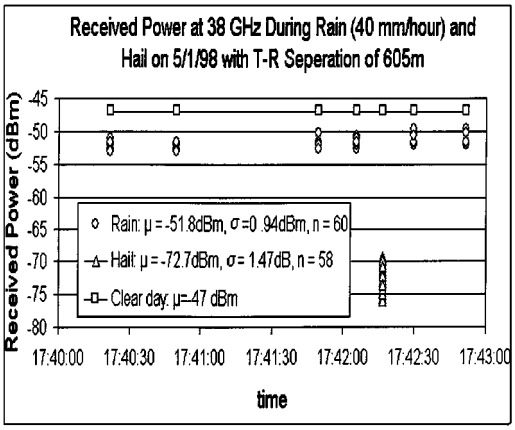

Fig. 9. Hail attenuation measurement: May 1, 605 m unobstructed LOS link, hail diameter of 0.5–1 cm.

a calm, sunny day. The measured mean attenuation due to the dry leaves of a single oak tree is 17 dB.

V. A Geometrically Based Millimeter-Wave Multipath Channel Model

A. General Description of the Model

Based on the high variability of reflections, a "worst case" method was devised to predict the maximum multipath delay or multipath power that could arise in a LMDS link. A prediction method for multipath channel characteristics is given in [21] based on a two-dimensional geometrical LOS model with omnidirectional antennas. The model developed in this work is a generalized three-dimensional model appropriate for any antenna.

The geometry of the model is depicted in Fig. 10, where the LOS path length is D, and a scatterer is located at (x_0, y_0, z_0). The scatterer may be a building wall, a rooftop, ground, or any object that has a large reflecting surface relative to the wavelength, which is on the order of millimeters for LMDS (at 38 GHz, for example, the wavelength is only 7.9 mm). The power of the wave reflected by the scatterer is dependent on polarization, angle of incidence, dielectric properties and surface roughness [22]. When highly directional antennas are used, strong multipath components are caused only by scatterers close to the LOS path. When the angle between the incident wave and the reflecting surface is very small (i.e., at grazing angle), effects of the surface roughness are negligible, and the reflection coefficient has an amplitude close to 1 [22]. At different incident angles, as shown in Section IV-A2, the surface appears more reflective when it becomes wet. For a worst case scenario, which is appropriate for equalizer design specification, each scatterer is assumed to be a perfect reflector with a reflection coefficient of 1. Practical reflection coefficients can be then taken into account based on this worst case model (Section V-C). A similar approach was also used in [23] to model street-level propagation at 55 GHz.

Under the assumption that the scatterer is a large perfect reflector, the relative received power, ΔP_{MP}, and excess delay time, τ_{MP}, of each multipath component are computed as follows:

$$\tau_{\mathrm{MP}} = (d_1 + d_2 - D)/c \,(\mathrm{s}) \tag{16}$$

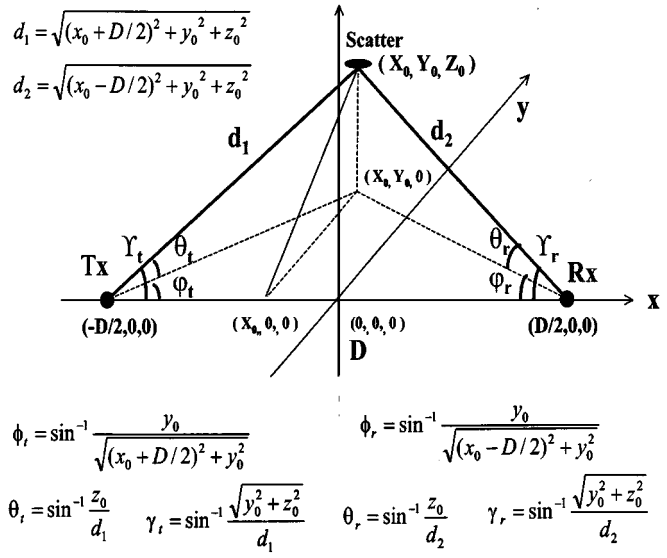

Fig. 10. Geometry of the model.

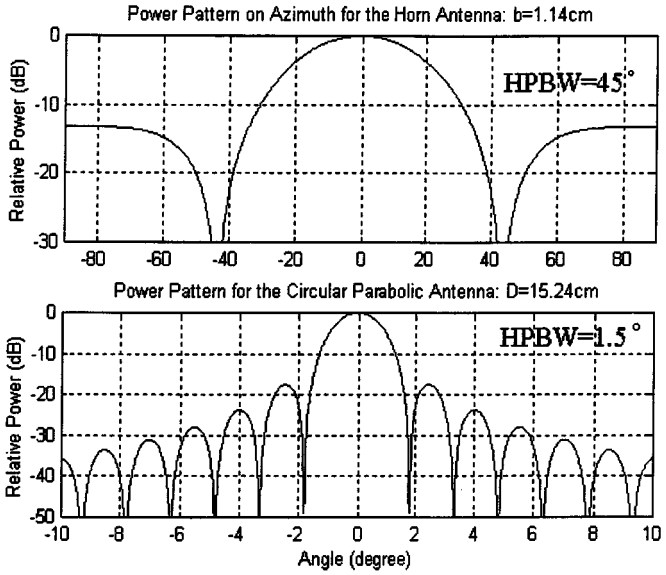

Fig. 11. Theoretical power patterns for horn and dish antennas: Azimuth.

$$\Delta P_{\mathrm{MP}} = G_t(\phi_t, \theta_t) + G_r(\phi_r, \theta_r) - (PL(d_1 + d_2) - PL(D)) \ (\mathrm{dB}) \tag{17}$$

where

- d_1 distance from the reflector to the transmitter;
- d_2 distance from the reflector to the receiver;
- c speed of light;
- G_t normalized antenna power patterns for transmitter;
- G_r normalized antenna power patterns for receiver.

$(PL(d_1 + d_2) - PL(D))$ accounts for the excess free space path loss associated with the path length difference between the reflected path and LOS path, and ϕ_t, θ_t, ϕ_r, θ_r are given in Fig. 11. Given a path length D and the location of the reflector (x_0, y_0, z_0), all the other parameters can be determined using the geometry shown in Fig. 10.

The model is demonstrated for following canonical antenna system: the uniformly illuminated rectangular aperture antenna as the transmitting antenna and the uniformly illuminated circular aperture antenna as the receiving antenna. The normalized far-field radiation power patterns, $G_t(\phi_t, \theta_t)$ and $G_r(\phi_r, \theta_r)$, for these antennas are given in [24] as follows:

$$G_t(\phi_t, \theta_t) = \left| \frac{\sin[\pi(a/\lambda)\sin(\phi)]\sin[\pi(b/\lambda)\sin(\theta)]}{\pi^2(ab/\lambda^2)\sin(\phi)\sin(\theta)} \right|^2 \tag{18}$$

where

- λ wavelength;
- a and b dimensions of the rectangular aperture;

$$G_r(\gamma_r) = |\pi r^2 2J_1(\xi)/\xi|^2 \tag{19}$$

where

- ξ $= 2\pi(r_0/\lambda)\sin(\gamma_r)$;
- J_1 first-order Bessel function;
- γ_r angle in spherical coordinate system as shown in Fig. 10.

Power patterns in azimuth plane are shown in Fig. 11. The theoretical antenna patterns provide excellent parametric approximations to the antennas used in this measurement campaign.

B. Relative Power Zone and Excess Delay Zone

We define the *relative power zone* as the region where a perfect reflector (with $\Gamma = 1$) would give rise to a multipath component whose power is within a certain range relative to LOS. Similarly, we define the *excess delay zone* as the region where a perfect reflector would give rise to a multipath component whose excess propagation delay is within a certain range of delay relative to LOS. Instead of calculating relative power and excess delay of multipath components caused by a scatterer in a given location, a more general approach applies the relative power zone and the excess delay zone.

For a certain excess delay τ_{MP}, the boundary of the excess delay zone given by (16) forms an ellipsoid. The closed form equation for the ellipsoid is

$$\frac{x_0^2}{K_t^2/4} + \frac{y_0^2}{K_t^2/4 - D^2/4} + \frac{z_0^2}{K_t^2/4 - D^2/4} = 1 \tag{20}$$

where $K_t = D + c * \tau_{MP}$ is a constant. It can be shown that the ratio of x and y axes of the ellipse changes with distance D and is given by $K_t/\sqrt{K_t^2 - D^2}$. An example of the excess delay zones is depicted in Fig. 12 for a path length of 1000 m. The contours represent excess delay zone boundaries.

Similarly, for a certain relative power level ΔP_{MP}, the relative power zone is given by (17). The resulting relative power zones for the canonical antennas are presented in Fig. 13, where the contours represent the power zone boundaries.

The excess delay zone plot and the relative power zone plot provide a simple but effective way to identify worst case multipath characteristics for any millimeter-wave point-to-point deployment. By overlaying the plots onto a site map and identifying potential scatterers, engineers can quickly estimate the delay and power of possible multipath components. For instance, if a building with a smooth surface is located on the 10-ns contour line (of the excess delay zone plot) and the –20-dB contour line (of the relative power zone plot), then the worst case estimate of the multipath power and arrival time from this scatterer are –20 dB and 10 ns relative to LOS. The worst case mean excess delay and rms delay spread for this

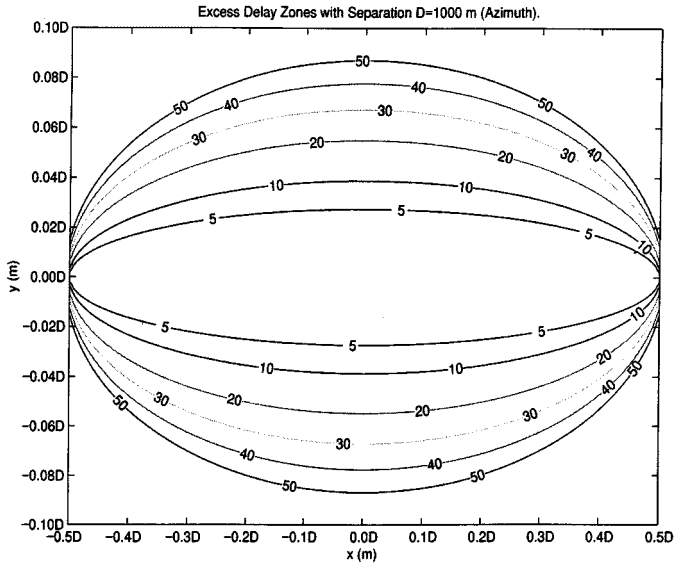

Fig. 12. The excess delay contour plot: for any antennas, $D = 1000$ m, Azimuth plane, $\Gamma = 1$, all units in ns.

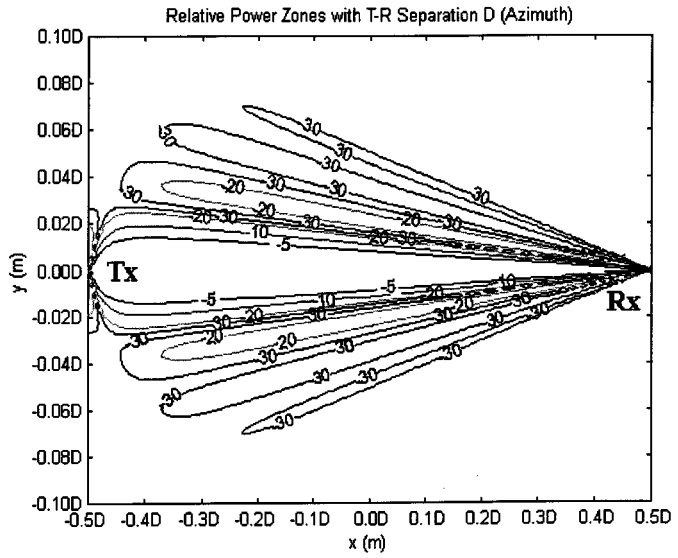

Fig. 13. The relative power contour plot: for horn and parabolic antennas, for any D, Azimuth plane, $\Gamma = 1$, all units in dB.

case are 0.1 and 0.99 ns, respectively. Angles of arrival, θ_r and ϕ_r, are calculated based on geometry from the contour plots.

The maximum radii of excess delay zone and relative power zone can be analytically determined from LOS path length D, expected delay $\tau_{\rm MP}$, and expected power $\Delta P_{\rm MP}$. From (20), maximum radius of an excess delay zone, $y_{dz}^{\max}$, is given by

$$y_{dz}^{\max} = \sqrt{K_t^2/4 - D/4} = \sqrt{(D + c * \tau_{\rm MP})^2/4 - D^2/4} \tag{21}$$

where $\tau_{\rm MP}$ is in seconds and D is in meters. Table V shows maximum excess delay zone radii for typical D and τ_{MP}.

The maximum radii of relative power zones, $y_{pz}^{\max}$, are evaluated using (17). The results are shown in Table V. Results show that $y_{pz}^{\max}$ is proportional to D. This is expected. When directive antennas are used for short-hop links, most of the energy is concentrated near the LOS path. Therefore, in (17), term

TABLE V
MAXIMUM RADII OF RELATIVE POWER ZONE AND EXCESS DELAY ZONE FOR HORN AND PARABOLIC ANTENNAS

D	Maximum Relative Power Zone Radii (m)				
ΔP_{MP}	5 dB	10 dB	20 dB	30 dB	35 dB
500 m	7	10	19	35	46
1 km	14.5	19.5	38.5	70	92
2km	29	39	77	140	185
5km	72	96	192	352	461
	Maximum Excess Delay Zone Radii (m)				
τ_{MP}	10 ns	20 ns	30 ns	40 ns	50 ns
500 m	27.4	38.8	47.6	55.1	61.7
1 km	38.8	54.9	67.2	77.7	86.9
2 km	54.8	77.5	95.0	109.7	122.7
3 km	67.1	94.9	116.3	134.3	150.2
4 km	77.5	109.6	134.2	155.0	173.4
5 km	86.6	122.5	150.1	173.3	193.8

$(PL(d_1+d_2) - PL(D))$ is negligibly small and relative power zones are mainly dependent on the antenna patterns.

Exact relationship between $y_{pz}^{\max}$ and $\Delta P_{\rm MP}$ requires solution of Bessel function and $\sin c$ function from (18) and (19), however, a polynomial fit can be applied to the results from Table V. This results in (22)

$$y_{pz}^{\max} = \frac{D}{1000}(0.07\Delta P_{\rm MP}^2 - 0.1947 * \Delta P_{\rm MP} + 12.6311) \text{ m} \tag{22}$$

where D is in meters and ΔP_{MP} is in decibels.

Equations (21) and (22) provide closed-form estimates of the worst case delay and power of multipath from a scatterer and can greatly simplify LMDS site planning and deployment.

C. Comments Regarding the Model

The excess delay contour plot in Fig. 12 is generated for a path length of 1000 m independent of antenna types. The relative power contour plot in Fig. 13 is developed using canonical antennas for any distance D. Using (17) and (20), one can easily develop plots for other path lengths and all types of antennas.

Second, the excess delay zones and relative power zones are spatial fields in three dimensions. Due to its radial symmetry about LOS path, the excess delay zone can be applied to any point in space. However, since the antenna patterns are generally not symmetric, the relative power zones in azimuth and elevation planes are different. Therefore, one should also develop relative power zones for the elevation plane. For any given point in the space, it is possible to find the projections onto these orthogonal planes. The power of the received multipath component is approximated by the sum of powers (in decibels) in each plane.

Third, the relative power zone and excess delay zone have interesting relationships with Fresnel zone. In fact, the excess delay zone can be viewed as a macro-Fresnel zone, where the distance between two successive zone boundaries gives rise to a particular propagation delay. A 1-ns delay corresponds to

0.3-m path difference, or 38 wavelengths at 38 GHz. Therefore, the excess delay zone boundaries are much larger than the Fresnel zone boundaries. For the specified antennas and a path length of 1000 m, the 760th Fresnel zone, 10 ns relative delay zone, and –20-dB relative power zone all have approximately the same maximum coverage. Excess delay zones and relative power zones, however, provide direct information about the worst case multipath power and delay.

Fourth, the model is developed for the case where the reflection coefficient is one. This provides a worst case estimate when no information for the reflection coefficient of a potential scatterer is available. Realistic reflection coefficients can be measured or estimated using site-specific information. If the reflection coefficient Γ is known, then the reflection loss is given by $L_{\text{reflect}} = 10\log_{10}|\Gamma|^2$. This loss can be added to the model by simply adjusting the power levels of the relative power zones in Fig. 13 by the value of L_{reflect}.

Finally, the model assumes that each multipath component is the result of a single reflection. Ray tracing can be applied to account for higher orders of reflection. The contour plots may be used to define the environment necessary for ray tracing. For instance, if the system requires that all multipath components have a relative power less than –10 dB, then the ray tracing environment only needs to include those features within the –10 dB relative power zone, thereby reducing the complexity of the ray tracing model.

VI. Conclusion

This paper presented the results of a wide-band measurement campaign performed on three point-to-point links at 38 GHz. The purpose of the research was to study the effects of various weather events such as rain and hail on the behavior of the broadband millimeter-wave channel. The measured links included a 605 m unobstructed LOS link, a 265 m obstructed link and a 265 m partially obstructed link. PDP's were recorded at a rate of 50 PDP's per second, and weather conditions were recorded every minute. During the campaign, 73 963 PDP were collected, of which 36 338 PDP's were collected during rain or hail.

Time dispersion of the channel was analyzed for different weather events. Multipath statistics shows that while very few multipath components were detected in clear, dry weather, more multipath components were detected during rain. These multipath statistics, summarized in Tables III and IV, provide insight into the design of equalizers and the selection of modulation techniques.

The short-term signal variation was analyzed for 1–2 min intervals at constant rain rates. Results show that received signal variation during rain follows a Rician distribution. The relationship between Rician K factor and rain rate as given in (9) shows increased scattered power and decreased LOS power at high rain rates. These results can be used to determine system outage probability.

Weather effects on received signal power were analyzed in terms of mean attenuation. Upper bounds of the mean attenuation were provided based on a modified Crane model in (14) and (15) for both unobstructed and partially obstructed links as functions of rain rate and path length. These upper bounds allow radio engineers to determine the additional fade margin necessary for the reliable operation of wide-band communication systems at millimeter-wave frequencies. Averaged attenuation in a hailstorm was measured to be 25.7 dB over the 605 m path.

Controlled reflection measurements on glass and brick surfaces showed that the specular reflection can increase by as much as 6.8 dB when the surface is wet. Attenuation measurements showed 17-dB attenuation through dense canopy of an oak tree, and 25.5 dB through a double-pane, tempered, and tinted window glass.

Finally, a deterministic approach was developed to facilitate the analysis of the multipath power, TOA, and AOA in a LOS millimeter-wave system. Through the use of the *relative power zones*, the *excess delay zones*, and system performance requirements, this approach greatly simplifies propagation prediction for millimeter-wave links. By applying the excess delay zone plot and the relative power zone plot to a site map, system engineers can identify potential reflectors and estimate worst case multipath characteristics.

Acknowledgment

The authors would like to thank R. Lovestead for his help in data processing, Prof. D.A. de Wolf, Prof. G. Brown, G. Durgin for helpful suggestions, and N. Patwari, P. Cardieri, Y. Ou, C. Garrison-Laney and C. Westcott for their help during the measurement campaign. The authors also wish to thank the reviewers for their valuable technical suggestions.

References

[1] O. Andrisano, V. Tralli, and R. Verdone, "Millimeter maves for short-range multimedia communication systems," *Proc. IEEE*, vol. 86, pp. 1383–1401, July 1998.

[2] L. Correia and R. Prasad, "An overview of wireless broadband communications," *IEEE Commun. Mag.*, pp. 28–33, Jan 1997.

[3] R. L. Freeman, *Radio System Design for Telecommunications (1–100 GHz)*. New York: Wiley, 1987.

[4] R. K. Crane, *Electromagnetic Wave Propagation Through Rain*. New York: Wiley, 1996.

[5] W. Rummler, "A new selective fading model: Application to propagation data," *Bell Syst. Tech. J.*, vol. 58, pp. 1037–1071, May–June 1979.

[6] P. Papazian, M. Roadifer, and G. Hufford, "Initial study of the local multipoint distribution system radio channel,", Tech. Rep. NTIA Rep. 94-315, Aug. 1994.

[7] S. Seidel and H. Arnold, "Propagation measurements at 28 GHz to investigate the performance of local multipoint distribution service (LMDS)," in *Proc. IEEE GLOBECOM*, 1995, pp. 754–757.

[8] E. Violette, R. Espeland, and K. Allen, "Millimeter-wave propagation characteristics and channel performance for urban-suburban environments,", Tech. Rep. NTIA Rep. 88-239, Dec. 1988.

[9] F. Schwering, E. Violette, and R. Espeland, "Millimeter-wave propagation in vegetation: Experiments and theory," *IEEE Trans. Geosci. Remote Sensing*, vol. 26, pp. 355–367, May 1988.

[10] D. Jones, R. Espeland, and E. Violette, "Vegetation loss measurements at 9.6, 28.8, 57.6, and 96.1 GHz through a conifer orchard in Washington state,", Tech. Rep. NTIA Rep. 89-251, Oct. 1989.

[11] S. Lin, "Statistical behavior of rain attenuation," *Bell Syst. Tech. J.*, vol. 52, pp. 557–581, Apr. 1973.

[12] K. H. Craig, M. P. M. Hall, J. R. Norbury, A. Seville, M. J. Willis, J. A. Biddiscombe, and T. G. Hayton, "Propagation research for millimeter wave cellular systems," in *IEE 10th Int. Conf. Antennas Propagat.*, Apr. 1997, pp. 2.383–2.386.

[13] M. Thurai and J. Woodroffe, "Precipitation induced co and cross-polar effects from a 9 km link operating at 38 GHz," in *IEE 10th Int. Conf. Antennas Propagat.*, Apr. 1997, pp. 2.222–2.225.

[14] T. Tjelta, A. Nordbotten, and J. Karstad, "Effects of precipitation and reflections from a snow covered ground measured at 40 and 60 GHz on a 600 m experimental link in Norway," in *IEE 10th Int. Conf. Antennas Propagat.*, Apr. 1997, pp. 2.234–2.238.

[15] H. Xu, R. Boyle, T. Rappaport, and J. Schaffner, "Radio wave propagation study at 38 GHz," in *Proc. IEEE VTC*, May 1999.

[16] D. C. Cox, "Delay Doppler characteristics of multipath delay spread and average excess delay for 910 Mhz urban mobile radio paths," *IEEE Trans. Antennas Propagat.*, vol. AP-20, pp. 625–635, Sept. 1972.

[17] W. Newhall, T. Rappaport, and D. Sweeney, "A spread spectrum sliding correlator system for propagation measurements," *RF Design*, pp. 40–54, Apr. 1996.

[18] H. Xu, R. Boyle, T. Rappaport, J. Schaffner, and R. Lovestead, "Radio wave propagation study at 38 GHz," Virginia Tech, MPRG TR-98–5, Sept. 1998.

[19] D. de Wolf and L. Ligthart, "Multipath effects due to rain at 30–50 GHz frequency communication links," *IEEE Trans. Antennas Propagat.*, pp. 1132–1138, Aug. 1993.

[20] S. O. Rice, "Statistical properties of a sine wave plus random noise," *Bell Syst. Tech. J.*, vol. 27, pp. 109–157, Jan. 1948.

[21] J. Liberti and T. Rappaport, "A geometrically based model for line-of-sight multipath radio channels," *Proc. IEEE VTC*, pp. 844–848, Apr. 1996.

[22] J. Ogilvy, *Theory of Wave Scattering from Random Rough Surfaces*. New York: Adam Hilger, 1991.

[23] H. J. Thomas, R. S. Cole, and G. L. Siqueira, "An experimental study of the propagation of 55 GHz millimeter waves in an urban mobile radio environment," *IEEE Trans. Veh. Technol.*, vol. 43, pp. 140–146, Feb. 1994.

[24] M. Skolnik, *Introduction to Radar Systems*, 2nd ed. New York: McGraw-Hill, 1980.

[25] H. Xu, T. Rappaport, R. Boyle, and J. Schaffner, "38 GHZ wideband point-to-multipoint measurements under different weather conditions," *IEEE Commun. Lett.*, pp. 7–8, Jan. 2000.

Hao Xu (S'96) was born in Wuhan, China, on February 28, 1971. He received the B.S.E.E. and M.S.E.E. degrees from Moscow Power Engineering Institute and Technical University, Moscow, Russia, in 1994 and 1996, respectively. In 1996, he began working toward the Ph.D. degree at the Mobile and Portable Radio Research Group (MPRG), Virginia Polytechnic Institute and State University, Blacksburg, where his research focuses are radio wave propagation, RF channel modeling, and wide-band spread spectrum system design. His current research includes millimeter-wave propagation at 38 and 60 GHz.

Mr. Xu received the IEEE Communications Society Stephen O. Rice Prize Paper Award in 1999. In 1989, as a result of his third place ranking in the national entrance examination to universities in China, he received the Zhang Zhongzhi Price Award from the University of Science and Technology of China, and Government Fellowship to study in Moscow. He is a member of Eta Kappa Nu.

Theodore S. Rappaport (S'83–M'84–SM'91–F'98) received the B.S.E.E., M.S.E.E., and Ph.D. degrees from Purdue University, West Lafayette, IN, in 1982, 1984, and 1987, respectively.

Since 1988, he has been on the electrical and computer engineering faculty of Virginia Polytechnic Institute and State University, Blacksburg, where he is the James S. Tucker Professor and Founding Director of the Mobile and Portable Radio Research Group (MPRG), a university research and teaching center dedicated to the wireless communications field. In 1989, he founded TSR Technologies, Inc., a cellular radio/PCS manufacturing firm that he sold in 1993. He has authored, coauthored, or coedited 14 books in the wireless field, including the popular textbook *Wireless Communications: Principles & Practice* (New York: Prentice-Hall, 1996), *Smart Antennas for Wireless Communications: IS-95 and Third Generation CDMA Applications* (New York: Prentice-Hall, 1999), and several compendia of papers, including *Cellular Radio & Personal Communications: Selected Readings* (New York: IEEE Press, 1995), *Cellular Radio & Personal Communications: Advanced Selected Readings* (New York: IEEE Press, 1996), and *Smart Antennas: Selected Readings* (New York: IEEE Press, 1998). He has coauthored more than 130 technical journal and conference papers, including the paper that received the 1999 IEEE Communications Society Stephen O. Rice Paper Award, and holds three patents. He has consulted for more than 20 multinational corporations and has served the International Telecommunications Union as a consultant for emerging nations.

Dr. Rappaport received the Marconi Young Scientist Award in 1990 and an NSF Presidential Faculty Fellowship in 1992. He serves on the editorial board of *International Journal of Wireless Information Networks* (New York: Plenum), and is active in the IEEE Communications and Vehicular Technology societies. He is also Chairman of Wireless Valley Communications, Inc., a microcell and in-building design and development firm. He is a registered professional engineer in the state of Virginia and is a Fellow and past member of the Board of Directors of the Radio Club of America.

Robert J. Boyle received the B.S. degree from the State University of New York, Buffalo, in 1984, and the M.S. and D.Sc. degrees from the George Washington University, Washington, DC, in 1990 and 1993, respectively.

From 1983 to 1984, he was with the Calspan Advance Technology Center working on signal processing techniques for airborne electronic warfare applications. From 1984 to 1988, he served as a signal officer in the U.S. Army where he was responsible for the development and procurement of tactical signals intelligence/electronic warfare systems and achieved the rank of Captain. In 1988, he joined E-Systems (now part of Raytheon) where he focused on the area signal processing for military intelligence systems. In 1993, he joined Comsearch and worked in the area of planning tool development and analysis for wireless communication systems. In 1994, he cofounded Radio Dynamics Corporation, a start-up company that focused on interference issues in cellular and PCS systems as well as spectrum sharing issues in heterogeneous wireless communication environments. In 1998, he joined the faculty of Virginia Polytechnic Institute and State University, Blacksburg, as a Research Assistant Professor. His research interests include smart antennas, equalization, sequence estimation, and space-time processing. His interests also include software radio design issues and the simulation of wireless communication systems at both the link and network levels.

James H. Schaffner (S'94–M'79–SM'97) received the B.S., M.S., and Ph.D. degrees in electrical engineering from UCLA in 1978, 1979, and 1988, respectively.

From 1978 to 1988, he was with the Hughes Aircraft Company Missile System Group, where he worked on microwave- and millimeter-wave antenna arrays, antenna feed networks, and MMIC circuits for transmit/receive modules. Since 1988, he has been a Senior Research Scientist at HRL Laboratories, Malibu, CA. Since joining HRL Laboratories, he has been active in research and development projects on high-speed and high-frequency fiber optic components and links, broadband, millimeter-wave wireless radio channel characterization and deployment, and RF microelectromechanical switch applications for antennas. He has coauthored 14 technical journal papers, and holds eight patents.